2

Constraining the Couplings of a Charged Higgs to Heavy Quarks

A. S. Cornell
National Institute for Theoretical Physics;
School of Physics, University of the Witwatersrand
South Africa

1. Introduction

The Standard Model (SM) of particle physics has been an incredibly successful theory which has been confirmed experimentally many times, however, it still has some short-comings. As such physicists continue to search for models beyond the SM which might explain issues such as naturalness (the hierarchy problem). Among the possible discoveries that would signal the existence of these new physics models (among several) would be the discovery of a charged Higgs boson.

Recall that in the SM we have a single complex Higgs doublet, which through the Higgs mechanism, is responsible for breaking the Electroweak (EW) symmetry and endowing our particles with their mass. As a result we expect one neutral scalar particle (known as the Higgs boson) to emerge. Now whilst physicists have become comfortable with this idea, we have not yet detected this illusive Higgs boson. Furthermore, this approach leads to the hierarchy problem, where extreme fine-tuning is required to stabilise the Higgs mass against quadratic divergences. As such a simple extension to the SM, which is trivially consistent with all available data, is to consider the addition of extra $SU(2)$ singlets and/or doublets to the spectrum of the Higgs sector. One such extension shall be our focus here, that where we have two complex Higgs doublets, the so-called Two-Higgs Doublet Models (2HDMs). Such models, after EW symmetry breaking, will give rise to a charged Higgs boson in the physical spectrum. Note also that by having these two complex Higgs doublets we can significantly modify the Flavour Changing Neutral Current (FCNC) Higgs interactions in the large $\tan\beta$ region (where $\tan\beta \equiv v_2/v_1$, the ratio of the vacuum expectation values (vevs) of the two complex doublets).

Among the models which contain a second complex Higgs doublet one of the best motivated is the Minimal Supersymmetric Standard Model (MSSM). This model requires a second Higgs doublet (and its supersymmetric (SUSY) fermionic partners) in order to preserve the cancellation of gauge anomalies [1]. The Higgs sector of the MSSM contains two Higgs supermultiplets that are distinguished by the sign of their hypercharge, establishing an unambiguous theoretical basis for the Higgs sector. In this model the structure of the Higgs sector is constrained by supersymmetry, leading to numerous relations among Higgs masses and couplings. However, due to supersymmetry-breaking effects, all such relations are modified by loop-corrections, where the effects of supersymmetry-breaking can enter [1].

Thus, one can describe the Higgs-sector of the (broken) MSSM by an effective field theory consisting of the most general 2HDM, which is how we shall develop our theory in section 2.

Note that in a realistic model, the Higgs-fermion couplings must be chosen with some care in order to avoid FCNC [2, 3], where 2HDMs are classified by how they address this: In type-I models [4] there exists a basis choice in which only one of the Higgs fields couples to the SM fermions. In type-II [5, 6], there exists a basis choice in which one Higgs field couples to the up-type quarks, and the other Higgs field couples to the down-type quarks and charged leptons. Type-III models [7] allow both Higgs fields to couple to all SM fermions, where such models are viable only if the resulting FCNC couplings are small.

Once armed with a model for a charged Higgs boson, we must determine how this particle will manifest and effect our experiments. Of the numerous channels, both direct and indirect, in which its presence could have a profound effect, one of the most constraining are those where the charged Higgs mediates tree-level flavour-changing processes, such as $B \to \tau\nu$ and $B \to D\tau\nu$ [8]. As these processes have already been measured at B-factories, they will provide us with very useful indirect probes into the charged Higgs boson properties. Furthermore, with the commencement of the Large Hadron Collider (LHC) studies involving the LHC environment promise the best avenue for directly discovering a charged Higgs boson. As such we shall determine the properties of the charged Higgs boson using the following processes:

- **LHC:** $pp \to t(b)H^+$: through the decays $H^\pm \to \tau\nu$, $H^\pm \to tb$ ($b-t-H^\pm$ coupling).
- **B-factories:** $B \to \tau\nu$ ($b-u-H^\pm$ coupling), $B \to D\tau\nu$ ($b-c-H^\pm$ coupling).

The processes mentioned above have several common characteristics with regard to the charged Higgs boson couplings to the fermions. Firstly, the parameter region of $\tan\beta$ and the charged Higgs boson mass covered by charged Higgs boson production at the LHC ($pp \to t(b)H^+$) overlaps with those explored at B-factories. Secondly, these processes provide four independent measurements to determine the charged Higgs boson properties. With these four independent measurements one can in principle determine the four parameters related to the charged Higgs boson couplings to b-quarks, namely $\tan\beta$ and the three generic couplings related to the $b-i-H^\pm$ ($i=u,c,t$) vertices. In our analysis we focus on the large $\tan\beta$-region [9], where one can neglect terms proportional to $\cot\beta$, where at tree-level the couplings to fermions will depend only on $\tan\beta$ and the mass of the down-type fermion involved. Hence, at tree-level, the $b-i-H^\pm$ ($i=u,c,t$) vertex is the same for all the three up-type generations. This property is broken by loop corrections to the charged Higgs boson vertex.

Our strategy in this pedagogical study will be to determine the charged Higgs boson properties first through the LHC processes. Note that the latter have been extensively studied in many earlier works (see Ref.[10], for example) with the motivation of discovering the charged Higgs boson in the region of large $\tan\beta$. We shall assume that the charged Higgs boson is already observed with a certain mass. Using the two LHC processes as indicated above, one can then determine $\tan\beta$ and the $b-t-H^\pm$ coupling. Having an estimate of $\tan\beta$ one can then study the B-decays and try to determine the $b-(u/c)-H^\pm$ couplings from B-factory measurements. This procedure will enable us to measure the charged Higgs boson couplings to the bottom quark and up-type quarks [11].

The chapter will therefore be organised in the following way: In Section 2 we shall discuss the model we have considered for our analysis. As we shall use an effective field theory

derived from the MSSM, we will also introduce the relevant SUSY-QCD and higgsino-stop loop correction factors to the relevant charged Higgs boson fermion couplings. Using this formalism we shall study in section 3 the possibility of determining the charged Higgs boson properties at the LHC using $H^\pm \to \tau\nu$ and $H^\pm \to tb$. In Section 4 we shall present the results of B-decays, namely $B \to \tau\nu$ and $B \to D\tau\nu$, as studied in Ref.[8]. Finally, we shall combine the B-decay results with our LHC simulations to determine the charged Higgs boson properties (such as its mass, $\tan\beta$ and SUSY loop correction factors) and give our conclusions.

2. Effective Lagrangian for a charged Higgs boson

In this section we shall develop the general form of the effective Lagrangian for the charged Higgs interactions with fermions. As already discussed in the introduction of this chapter, at tree-level the Higgs sector of the MSSM is of the same form as the type-II 2HDM, also in (at least in certain limits of) those of type-III. In these 2HDMs the consequence of this extended Higgs sector is the presence of additional Higgs bosons in the physics spectrum. In the MSSM we will have 5 Higgs bosons, three neutral and two charged.

2.1 The MSSM charged Higgs

We shall begin by recalling that we require at least two Higgs doublets in SUSY theories, where in the SM the Higgs doublet gave mass to the leptons and down-type quarks, whilst the up-type quarks got their mass by using the charge conjugate (as was required to preserve all gauge symmetries in the Yukawa terms). In the SUSY case the charge conjugate cannot be used in the superpotential as it is part of a supermultiplet. As such the simplest solution is to introduce a second doublet with opposite hypercharge. So our theory will contain two chiral multiplets made up of our two doublets H_1 and H_2 and corresponding higgsinos $\widetilde{H}_1$ and $\widetilde{H}_2$ (fields with a tilde ($\widetilde{}$) denote squarks and sleptons); in which case the superpotential in the MSSM is:

$$W = -H_1 D^c \mathbf{y}_d Q + H_2 U^c \mathbf{y}_u Q - H_1 E^c \mathbf{y}_e L + \mu H_1 H_2 \,. \tag{1}$$

The components of the weak doublet fields are denoted as:

$$H_1 = \begin{pmatrix} H_1^0 \\ H_1^- \end{pmatrix} \,,\; H_2 = \begin{pmatrix} H_2^+ \\ H_2^0 \end{pmatrix} \,,\; Q = \begin{pmatrix} U \\ D \end{pmatrix} \,,\; L = \begin{pmatrix} N \\ E \end{pmatrix} \,. \tag{2}$$

The quantum numbers of the $SU(3) \times SU(2) \times U(1)$ gauge groups for H_1, H_2, Q, L, D^c, U^c, E^c are $(\mathbf{1},\mathbf{2},-1)$, $(\mathbf{1},\mathbf{2},1)$, $(\mathbf{3},\mathbf{2},\frac{1}{3})$, $(\mathbf{1},\mathbf{2},-1)$, $(\mathbf{3},\mathbf{1},\frac{2}{3})$, $(\mathbf{3},\mathbf{1},-\frac{4}{3})$, $(\mathbf{1},\mathbf{1},2)$; where the gauge and family indices were eliminated in Eq.(1). For example $\mu H_1 H_2 = \mu (H_1)_\alpha (H_2)_\beta \epsilon^{\alpha\beta}$ with $\alpha, \beta = 1,2$ being the $SU(2)_L$ isospin indices and $H_1 D^c \mathbf{y}_d Q = (H_1)_\beta D^{ci}_a (\mathbf{y}_d)^j_i Q^a_{j\alpha} \epsilon^{\alpha\beta}$ with $i, j = 1,2,3$ as the family indices and $a = 1,2,3$ as the colour indices of $SU(3)_c$. As in the SM the Yukawas $\mathbf{y}_d$, $\mathbf{y}_u$ and $\mathbf{y}_e$ are 3×3 unitary matrices.

Note that Eq.(1) does not contain terms with H_1^* or H_2^*, consistent with the fact that the superpotential is a holomorphic function of the supermultiplets. Yukawa terms like $\bar{U} Q H_1^*$, which are usually present in non-SUSY models, are excluded by the invariance under the supersymmetry transformation.

The soft SUSY breaking masses and trilinear SUSY breaking terms (A-term) are given by:

$$\begin{aligned}\mathcal{L}_{\rm soft} = &-\widetilde{Q}_{\rm L}^{\dagger} M^2_{\widetilde{Q}_{\rm L}} \widetilde{Q}_{\rm L} - \widetilde{U}_{\rm R}^{\dagger} M^2_{\widetilde{U}_{\rm R}} \widetilde{U}_{\rm R} - \widetilde{D}_{\rm R}^{\dagger} M^2_{\widetilde{D}_{\rm R}} \widetilde{D}_{\rm R} - \widetilde{L}_{\rm L}^{\dagger} M^2_{\widetilde{L}_{\rm L}} \widetilde{L}_{\rm L} - \widetilde{E}_{\rm R}^{\dagger} M^2_{\widetilde{E}_{\rm R}} \widetilde{E}_{\rm R} \\ &+ H_1 \widetilde{D}_{\rm R}^{\dagger} \mathbf{A}_d \widetilde{Q}_{\rm L} - H_2 \widetilde{U}_{\rm R}^{\dagger} \mathbf{A}_u \widetilde{Q}_{\rm L} + H_1 \widetilde{E}_{\rm R}^{\dagger} \mathbf{A}_e \widetilde{L}_{\rm L} + {\rm h.c.} \end{aligned} \tag{3}$$

Let us first discuss the simplest case where soft breaking masses are proportional to a unit matrix in the flavour space, and $\mathbf{A}_u, \mathbf{A}_d$ and $\mathbf{A}_e$ are proportional to Yukawa couplings. Their explicit forms being:

$$\begin{aligned} &M^2_{\widetilde{Q}_{{\rm L}ij}} = a_1 \widetilde{M}^2 \delta_{ij} \ , \ M^2_{\widetilde{U}_{{\rm R}ij}} = a_2 \widetilde{M}^2 \delta_{ij} \ , \ M^2_{\widetilde{D}_{{\rm R}ij}} = a_3 \widetilde{M}^2 \delta_{ij} \ , \ M^2_{\widetilde{L}_{{\rm L}ij}} = a_4 \widetilde{M}^2 \delta_{ij} \ , \\ &M^2_{\widetilde{E}_{{\rm R}ij}} = a_5 \widetilde{M}^2 \delta_{ij} \ , \ \mathbf{A}_{uij} = A_u \mathbf{y}_{uij} \ , \ \mathbf{A}_{dij} = A_d \mathbf{y}_{dij} \ , \ \mathbf{A}_{eij} = A_e \mathbf{y}_{eij} \ , \end{aligned} \tag{4}$$

where $a_i (i = 1 - 5)$ are real parameters.

At tree-level the Yukawa couplings have the same structure as the above superpotential, namely, H_1 couples to D^c and E^c, and H_2 to U^c. On the other hand, different types of couplings are induced when we take into account SUSY breaking effects through one-loop diagrams. The Lagrangian of the Yukawa sector can be written as:

$$\begin{aligned}\mathcal{L}_{\rm Yukawa} = &-H_1 \overline{D}_{\rm R} \mathbf{y}_d Q_{\rm L} + H_2 \overline{U}_{\rm R} \mathbf{y}_u Q_{\rm L} - H_1 \overline{E}_{\rm R} \mathbf{y}_e L_{\rm L} - i\sigma_2 H_2^* \overline{D}_{\rm R} \Delta \mathbf{y}_d Q_{\rm L} \\ &+ i\sigma_2 H_1^* \overline{U}_{\rm R} \Delta \mathbf{y}_u Q_{\rm L} - i\sigma_2 H_2^* \overline{E}_{\rm R} \Delta \mathbf{y}_e L_{\rm L} + {\rm h.c.} \ , \end{aligned} \tag{5}$$

where $\Delta \mathbf{y}_d$, $\Delta \mathbf{y}_u$, and $\Delta \mathbf{y}_e$ are one-loop induced coupling constants, and we recall that gauge indices have been suppressed; for example $\sigma_2 H_2^* \overline{D}_{\rm R} \Delta \mathbf{y}_d Q_{\rm L} = (\sigma_2)^{\alpha\beta} (H_2^*)_\beta (\overline{D}_{\rm R})^i_a (\Delta \mathbf{y}_d)^j_i (Q_{\rm L})^a_{j\alpha}$. From the above Yukawa couplings, we can derive the quark and lepton mass matrices and their charged Higgs couplings. For the quark sector, we get

$$\begin{aligned}\mathcal{L}_{\rm quark} = &-\frac{v}{\sqrt{2}} \cos\beta \overline{D}_{\rm R} \mathbf{y}_d [1 + \tan\beta \Delta_{m_d}] D_{\rm L} + \sin\beta H^- \overline{D}_{\rm R} \mathbf{y}_d [1 - \cot\beta \Delta_{m_d}] U_{\rm L} \\ &-\frac{v}{\sqrt{2}} \sin\beta \overline{U}_{\rm R} \mathbf{y}_u [1 - \cot\beta \Delta_{m_u}] U_{\rm L} + \cos\beta H^+ \overline{U}_{\rm R} \mathbf{y}_u [1 + \tan\beta \Delta_{m_u}] D_{\rm L} + {\rm h.c.} \ , \end{aligned} \tag{6}$$

where we define $\Delta_{m_d} (\Delta_{m_u})$ as $\Delta_{m_d} \equiv \mathbf{y}_d^{-1} \Delta \mathbf{y}_d$ ($\Delta_{m_u} \equiv \mathbf{y}_u^{-1} \Delta \mathbf{y}_u$), and $v \simeq 246$GeV. Notice that $\Delta \mathbf{y}_d$ is proportional to $\mathbf{y}_d$ or $\mathbf{y}_d \mathbf{y}_u^\dagger \mathbf{y}_u$ in this case. We then rotate the quark bases as follows:

$$U_{\rm L} = V_{\rm L}(Q) U'_{\rm L} \ , \ D_{\rm L} = V_{\rm L}(Q) V_{\rm CKM} D'_{\rm L} \ , \ U_{\rm R} = V_{\rm R}(U) U'_{\rm R} \ , \ D_{\rm R} = V_{\rm R}(D) D'_{\rm R} \ , \tag{7}$$

where the fields with a prime ($'$) are mass eigenstates. In this basis, the down-type quark Lagrangian is given by

$$\begin{aligned}\mathcal{L}_{\rm D-quark} = &-\frac{v}{\sqrt{2}} \cos\beta \overline{D}_{\rm R}{}' V_{\rm R}^\dagger(D) \mathbf{y}_d V_{\rm L}(Q) \widehat{R}_d V_{\rm CKM} D'_{\rm L} \\ &+ \sin\beta H^- \overline{D}_{\rm R}{}' V_{\rm R}^\dagger(D) \mathbf{y}_d V_{\rm L}(Q) U'_{\rm L} + {\rm h.c.} \ , \end{aligned} \tag{8}$$

where $\widehat{R}_d \equiv 1 + \tan\beta \widehat{\Delta}_{m_d}$ and $\widehat{\Delta}_{m_d} \equiv V_{\rm L}^\dagger(Q) \Delta_{m_d} V_{\rm L}(Q)$. Hereafter, a matrix with a hat ($\widehat{\ }$) represents a diagonal matrix. Since the down-type diagonal mass term is given by

$$\widehat{M}_d \equiv \frac{v}{\sqrt{2}} \cos\beta V_{\rm R}^\dagger(D) \mathbf{y}_d V_{\rm L}(Q) \widehat{R}_d V_{\rm CKM} \ , \tag{9}$$

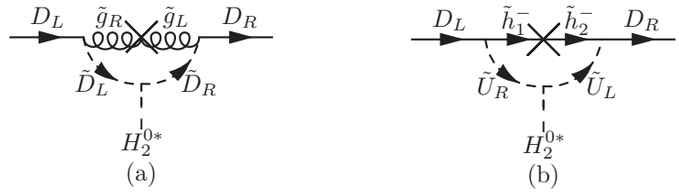

Fig. 1. Non-holomorphic radiative corrections to the down-type quark Yukawa couplings induced by (a) gluino $\widetilde{g}_{\mathrm{L,R}}$ and (b) charged higgsino $\widetilde{h}^-_{1,2}$.

we obtain the following Lagrangian for down-type quarks.

$$\mathcal{L}_{\mathrm{D-quark}} = -\overline{D}_{\mathrm{R}}{}'\widehat{M}_d D'_{\mathrm{L}} + \frac{\sqrt{2}}{v}\tan\beta H^- \overline{D}_{\mathrm{R}}{}'\widehat{M}_d V^\dagger_{\mathrm{CKM}}\widehat{R}_d^{-1}U'_{\mathrm{L}} + \mathrm{h.c.} \tag{10}$$

The corresponding corrections to the up-type couplings can be calculated from Eq.(6). Since we are interested in the large $\tan\beta$ case, these corrections are very small. In the following we neglect such corrections, and the Lagrangian for the up-type quarks is given as follows:

$$\mathcal{L}_{\mathrm{U-quark}} = -\overline{U}_{\mathrm{R}}{}'\widehat{M}_u U'_{\mathrm{L}} + \frac{\sqrt{2}}{v}\cot\beta H^+ \overline{U}_{\mathrm{R}}{}'\widehat{M}_u V_{\mathrm{CKM}} D'_{\mathrm{L}} + \mathrm{h.c.} \tag{11}$$

For the case of the charged-lepton, we can derive the relevant parts of the Lagrangian in a similar way to the case of the down-type quark by choosing an appropriate basis choice.

In the present case with Eqs.(4) $\widehat{\Delta}_{m_d}$ receives contributions from gluino and down-type squark, and higgsino and up-type squark diagrams. The explicit form is given as follows:

$$\widehat{\Delta}_{m_d} = \widehat{\mathbf{E}}_{\widetilde{g}} + \widehat{\mathbf{E}}_{\widetilde{h}}\,, \tag{12}$$

where

$$\widehat{\mathbf{E}}_{\widetilde{g}} \equiv \frac{2\alpha_s}{3\pi}\mathbf{1}\mu^* M_{\tilde{g}} I[M_{\tilde{g}}, M_{\tilde{D}_{\mathrm{L}}}, M_{\tilde{D}_{\mathrm{R}}}]\,, \tag{13}$$

$$\widehat{\mathbf{E}}_{\widetilde{h}} \equiv -\frac{\mu}{16\pi^2}A_{\mathrm{u}}|\widehat{\mathbf{y}}_{\mathrm{u}}|^2 I[M_{\widetilde{h}}, M_{\widetilde{U}_{\mathrm{L}}}, M_{\widetilde{U}_{\mathrm{R}}}]\,, \tag{14}$$

$$I[a,b,c] = \frac{a^2b^2\ln\frac{a^2}{b^2} + b^2c^2\ln\frac{b^2}{c^2} + c^2a^2\ln\frac{c^2}{a^2}}{(a^2-b^2)(b^2-c^2)(a^2-c^2)}\,. \tag{15}$$

$\widehat{\mathbf{E}}_{\widetilde{g}}$ and $\widehat{\mathbf{E}}_{\widetilde{h}}$ are gluino and charged higgsino contributions shown in Fig.1(a) and (b) respectively. Note that these corrections for Yukawa couplings are calculated in the unbroken phase of $\mathrm{SU}(2)\times\mathrm{U}(1)$.

Up to now we have assumed all squark mass matrices are proportional to a unit matrix at the EW scale, as shown in Eqs.(4). However, models with Minimal Flavour Violation (MFV) correspond to more general cases. For instance, the assumption of Eqs.(4) is not satisfied in minimal supergravity, where all squarks have a universal mass at the Planck scale, not at the EW scale. In Ref.[8] they derive the charged Higgs coupling in a more general case of MFV. Namely the squark mass matrix is taken to be

$$\begin{aligned} M^2_{\widetilde{Q}_{\mathrm{L}}} &= [a_1\mathbf{1} + b_1\mathbf{y}_u^\dagger\mathbf{y}_u + b_2\mathbf{y}_d^\dagger\mathbf{y}_d]\widetilde{M}^2\,,\\ M^2_{\widetilde{U}_{\mathrm{R}}} &= [a_2\mathbf{1} + b_5\mathbf{y}_u\mathbf{y}_u^\dagger]\widetilde{M}^2\,,\\ M^2_{\widetilde{D}_{\mathrm{R}}} &= [a_3\mathbf{1} + b_6\mathbf{y}_d\mathbf{y}_d^\dagger]\widetilde{M}^2\,. \end{aligned} \tag{16}$$

The final results of the charged Higgs coupling being given by

$$\mathcal{L}_{H^\pm} \approx \frac{\sqrt{2}}{v}\tan\beta H^- \overline{D}_{\mathrm{R}i}{}' \frac{\widehat{M}_{di}}{1+[E_{\widetilde{g}}{}^{(i)}]\tan\beta} V^\dagger_{\mathrm{CKM}ij} U'_{\mathrm{L}j} + \mathrm{h.c.}$$
$$\text{for } (i,j) = (1,1),(1,2),(2,1),(2,2), \tag{17}$$

$$\mathcal{L}_{H^\pm} \approx \frac{\sqrt{2}}{v}\tan\beta H^- \overline{D}_{\mathrm{R}i}{}' \frac{\widehat{M}_{di}}{1+[E_{\widetilde{g}}{}^{(i)} - E'_{\widetilde{g}}{}^{(ij)}]\tan\beta} V^\dagger_{\mathrm{CKM}ij} U'_{\mathrm{L}j} + \mathrm{h.c.}$$
$$\text{for } (i,j) = (3,1),(3,2), \tag{18}$$

$$\mathcal{L}_{H^\pm} \approx \frac{\sqrt{2}}{v}\tan\beta H^- \overline{D}_{\mathrm{R}i}{}' \frac{\widehat{M}_{di}}{1+E_{\widetilde{g}}{}^{(i)}\tan\beta} \frac{1+[E_{\widetilde{g}}{}^{(3)} + E_{\widetilde{h}}{}^{(33)}]\tan\beta}{1+[E_{\widetilde{g}}{}^{(i)} + E_{\widetilde{h}}{}^{(33)} + E'_{\widetilde{g}}{}^{(ij)} + E_{\widetilde{h}}{}^{(i3)} + E'_{\widetilde{h}}{}^{(i33)}]\tan\beta}$$
$$\times V^\dagger_{\mathrm{CKM}ij} U'_{\mathrm{L}j} + \mathrm{h.c.} \ \text{ for } (i,j) = (1,3),(2,3), \tag{19}$$

$$\mathcal{L}_{H^\pm} \approx \frac{\sqrt{2}}{v}\tan\beta H^- \overline{D}_{\mathrm{R}i}{}' \frac{\widehat{M}_{di}}{1+[E_{\widetilde{g}}{}^{(i)} + E_{\widetilde{h}}{}^{(i3)}]\tan\beta} V^\dagger_{\mathrm{CKM}ij} U'_{\mathrm{L}j} + \mathrm{h.c.}$$
$$\text{for } (i,j) = (3,3). \tag{20}$$

The functions $E_{\widetilde{g}}{}^{(i)}$, etc. are listed in Ref.[8]. In deriving these results only the y_t in the up-type Yukawa coupling in loop diagrams was kept and use made of the hierarchy of the CKM matrix elements. See Ref.[8] for details. Notice that the above results do not depend on the relationship between the A-terms and the Yukawa couplings, since only the y_t in loop diagrams was kept, even though Eqs.(4) are assumed.

2.2 Couplings to the bottom quark

From Eq.(10) and now under the assumption of MFV, we know that trilinear couplings are in general proportional to the original Yukawa couplings. We shall therefore label the components of the diagonal matrix $\widehat{R}_d^{-1} = \mathrm{diag}\left[R_{11}^{-1}, R_{22}^{-1}R_{33}^{-1}\right]$, where the three diagonal values of $\widehat{R}_d^{-1}$ represent the couplings of a charged Higgs boson to the bottom quark and the three up-type quarks. At tree-level, these three couplings are equal, $R_{11}^{-1} = R_{22}^{-1} = R_{33}^{-1} = 1$, where this equality is broken to some extent by loop corrections to the charged Higgs vertex, and $\widehat{R}_d$ can then be written as:

$$\widehat{R}_d = 1 + \tan\beta\hat{\Delta}_{m_d} \ . \tag{21}$$

In the forth-coming analysis we have kept the $\mathcal{O}(\alpha_s)$ SUSY-QCD corrections and SUSY loop corrections associated with the Higgs-top Yukawa couplings (as discussed in the previous subsection) and have neglected the subleading EW corrections of the order $\mathcal{O}(g^2)$ as given in Ref.[12].[1] Therefore, they then depend upon the higgsino-mass parameter μ, the up-type trilinear couplings A, and the bino, bottom and top squark masses. As argued in Ref.[8] the higgsino-diagram contributions can be neglected in R_{11}^{-1} and R_{22}^{-1}, so that to a very good approximation $R_{11}^{-1} \approx R_{22}^{-1}$. As an illustration, we show in Fig.2 the dependence of the SUSY corrections on $\tan\beta$ for some illustrative SUSY parameters. These corrections can alter the tree-level values significantly, although low-energy data (e.g. from $b \to s\gamma$, $B - \bar{B}$ mixing,

[1] For an alternative definition, in which SUSY loop effects are assigned to the CKM matrix, see Ref.[13]

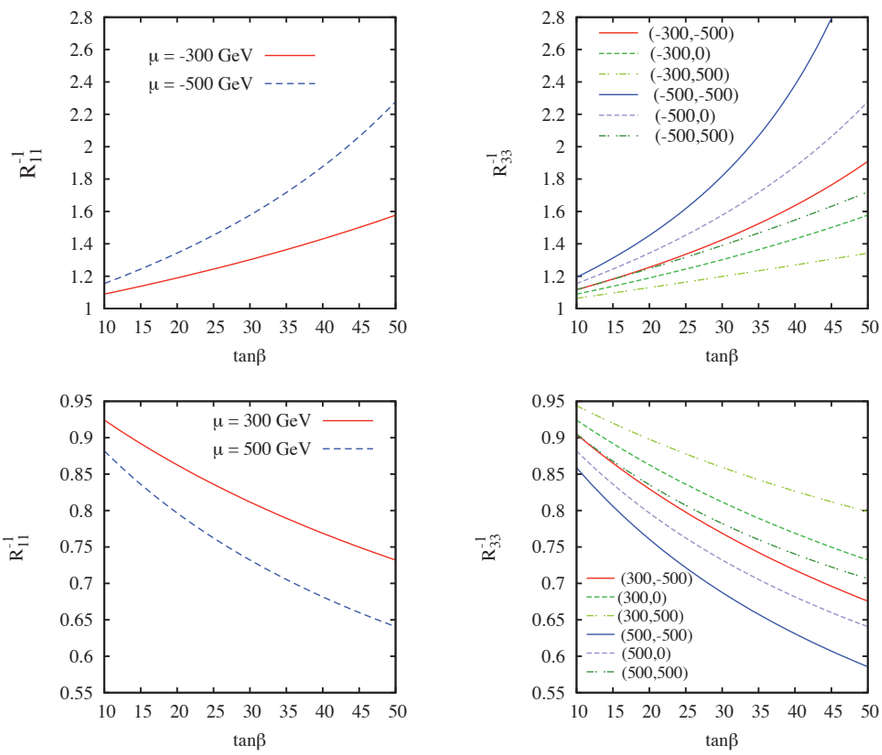

Fig. 2. Dependence of the general couplings R_{ii}^{-1} on $\tan\beta$ in the exemplary case of the MSSM for various values of the higgsino mass parameter μ and the up-type trilinear coupling A. The left-hand plots are for $R_{11}^{-1} = R_{22}^{-1}$, while those on the right are for R_{33}^{-1}. We present the case of negative μ in the top panels and for positive μ below. The other SUSY parameters are $M_{\tilde{g}}$ = 800 GeV and $M_{\tilde{b}_1} = M_{\tilde{t}_1} = 500$ GeV. We have also assumed $M_{\tilde{t}_L} = M_{\tilde{t}_R}$ and $M_{\tilde{b}_L} = M_{\tilde{b}_R}$. The legends in the right top and right bottom panels correspond to (μ, A) in GeV.

$B \to \mu\mu$ and $b \to s\mu\mu$) restricts the admissible parameter space [14]. In addition, it can be observed that the higgsino corrections are proportional to the up-type Yukawa couplings and hence can be substantial for diagrams involving the top quark as an external fermion line. This effectively implies that R_{33}^{-1} can differ substantially from R_{11}^{-1}, where for certain SUSY scenarios, as shown in Fig.2, we observe that R_{33}^{-1} can differ from R_{11}^{-1} by more than 30%. This difference could be observed at the LHC for processes that depend on R_{33}^{-1} when compared with the results of B-factories for processes that depend on R_{11}^{-1}. We remind the reader that the effective couplings are invariant under a rescaling of all SUSY masses and may indeed be the first observable SUSY effect, as long as the heavy Higgs bosons are light enough. The situation is similar in other models predicting a charged Higgs boson, such as those with a Peccei-Quinn symmetry, spontaneous CP violation, dynamical symmetry breaking, or those based on E_6 superstring theories, but these have usually been studied much less with respect to the constraints imposed by low-energy data. In the remainder of this work, we shall thus treat the diagonal entries of $\widehat{R}_d^{-1}$ as model-independent free parameters in our simulations and numerics, but we will assume that $R_{11}^{-1} \approx R_{22}^{-1}$. Note that the corresponding corrections to the up-type couplings are suppressed by $\cot\beta$ and hence can be neglected in our analysis.

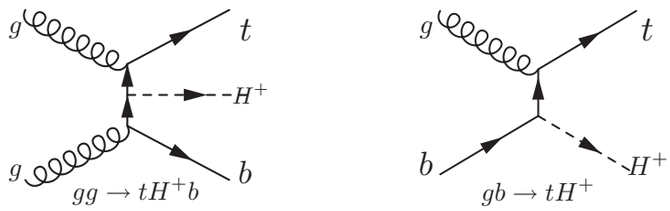

Fig. 3. The charged Higgs production at the LHC through the $gg \to tbH^{\pm}$ process, the $gb \to tH^{\pm}$ process, and there will also be parton level processes. The inclusive cross-section is the sum of these contributions, after the subtraction of common terms.

3. The $H^{\pm}$ decay channels at the LHC

With the theory for a charged Higgs coupling to heavy quarks now developed, we shall now consider the case where the charged Higgs boson is heavier than the top quark mass. Our reasoning for doing this, in this illustrative example, is that experimental searches have already placed a lower limit on the mass of a charged Higgs, including LEP, which set a limit of $m_{H^{\pm}} > 78.6$ GeV [15]. Note that within the MSSM, the charged Higgs mass is constrained by the pseudo-scalar Higgs mass and W-boson mass at tree level, with only moderate higher-order corrections, resulting in $m_{H^{\pm}} \gtrsim 120$ GeV. Furthermore, the Tevatron constrains (in several different MSSM scenarios) $m_{H^{\pm}} \gtrsim 150$ GeV [16], and at the LHC ATLAS has so far found (for $\tan\beta > 22$) $m_{H^{\pm}} > 140$ GeV [17] and CMS $m_{H^{\pm}} \gtrsim 160$ GeV [18].

As such, with $m_{H^{\pm}} \gtrsim m_t$, the production mechanism at the LHC shall be the associated production $pp \to tbH^{\pm} + X$ (the main production mechanisms are then $gg \to tbH^{\pm}$, $gb \to tH^{\pm}$ and the parton level processes, as shown in Fig.3[19]), with alternative production mechanisms like quark-antiquark annihilation, $q\bar{q} \to H^+H^-$[20] and $H^{\pm}+$ jet production, associated production with a W boson, $q\bar{q} \to H^{\pm}W^{\mp}$[21], or Higgs pair production having suppressed rates. Note that some of the above production processes may be enhanced in models with non-MFV, which we shall not consider here.

Once produced, it is expected that the decay channel $H^+ \to \tau\nu$ shall be the primary discovery channel for the charged Higgs boson. Recall that we shall consider the large $\tan\beta$ region, where the branching ratios of charged decays into SM particles is given in Fig.4[10]. For $\tan\beta = 40$ the branching ratio for $H^+ \to tb$ is also quite high, we shall therefore consider both decay channels here. Note that we have assumed a heavy SUSY spectrum, such that the charged Higgs will decay only into SM particles for the maximal stop mixing scenario. For low values of $\tan\beta$, below the top quark mass, the main decay channels are $H^{\pm} \to \tau^{\pm}\nu_{\tau}$, $c\bar{s}$, Wh^0 and t^*b.

As such we shall now simulate the charged Higgs boson in the LHC environment with as much care as is possible, where we have included QCD corrections, as well as fully analysing the $H^+ \to tb$ mode. We should note though that of the main production mechanisms in Fig.3, there will be a partial overlap when the $gb \to tH^{\pm}$ is obtained from the $gg \to tbH^{\pm}$ by a gluon splitting into a b-quark pair. The summing of both contributions must be done with care, so as to avoid double counting, as we shall now discuss in greater detail.

3.1 The resolution of double-counting and the normalisation of the cross-section

From the associated production $pp \to tbH^{\pm} + X$, two different mechanisms can be employed to calculate the production cross-section. The first is the four flavour scheme with no b quarks

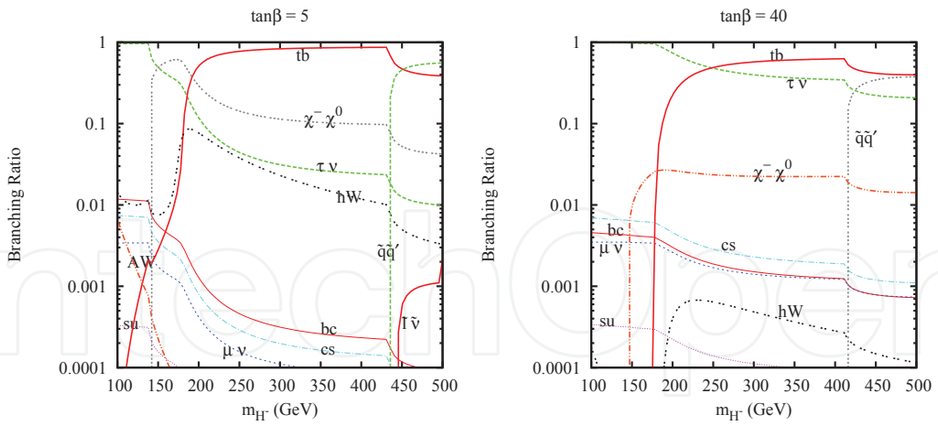

Fig. 4. The branching ratios of charged decays into SM particles as a function of $m_{H^\pm}$, for $\tan\beta = 5$ (left panel), and $\tan\beta = 40$ (right panel)[10].

in the initial state, the lowest order QCD production processes are gluon-gluon fusion and quark-antiquark annihilation, $gg \to tbH^\pm$ and $q\bar{q} \to tbH^\pm$ respectively. Note that potentially large logarithms $\propto \ln(\mu_F/m_b)$, arising from the splitting of incoming gluons into nearly collinear $b\bar{b}$ pairs, can be summed to all orders in perturbation theory by introducing bottom parton densities. This then defines the five flavour scheme. The use of bottom distribution functions is based on the approximation that the outgoing b quark is at small transverse momentum and massless, and the virtual b quark is quasi on-shell. In this scheme, the leading order process for the inclusive $tbH^\pm$ cross-section is gluon-bottom fusion, $gb \to tH^\pm$. The corrections to $gb \to tH^\pm$ and tree-level processes $gg \to tbH^\pm$ and $q\bar{q} \to tbH^\pm$. To all orders in perturbation theory the four and five flavour schemes are identical, but the way of ordering the perturbative expansion is different, and the results do now match exactly at finite order.

As such, in order to resolve the double-counting problem during event generation we use MATCHIG[22] as an external process to PYTHIA6.4.11[23]. In this program, when the $gb \to tH^-$ ($g\bar{b} \to \bar{t}H^+$) process is generated, there will be an accompanying outgoing $\bar{b}$ (b) quark. For low transverse momenta of this accompanying b quark, this process, including initial state parton showers, describes the cross-section well. However, for large transverse momentum of the accompanying b-quark one instead uses the exact matrix element of the $gg \to t\bar{b}H^-$ ($gg \to \bar{t}bH^+$) process. Whilst for low transverse momenta, this process can be described in terms of the gluon splitting to $b\bar{b}$ times the matrix element of the $gb \to tH^\pm$ process. As was shown in Ref.[24], for low transverse momenta ($\lesssim$ 100GeV) the $gg \to t\bar{b}H^\pm$ approach underestimates the differential cross-section. Therefore, when the accompanying b-quark is observed, it is necessary to use both the $g\bar{b} \to tH^\pm$ and the $gg \to t\bar{b}H^\pm$ processes together, appropriately matched to remove the double-counting.

To do this MATCHIG defines a double-counting term $\sigma_{\rm DC}$, given by the part of the $gg \to t\bar{b}H^\pm$ process which is already included in the $g\bar{b} \to tH^\pm$ process. This term is then subtracted from the sum of the cross-sections of the two processes. The double-counting term is given by the leading contribution of the b quark density as:

$$\sigma_{\rm DC} = \int dx_1 dx_2 \left[g(x_1,\mu_F) b'(x_2,\mu_F) \frac{d\widehat{\sigma}_{2\to 2}}{dx_1 dx_2}(x_1,x_2) + x_1 \leftrightarrow x_2 \right] , \tag{22}$$

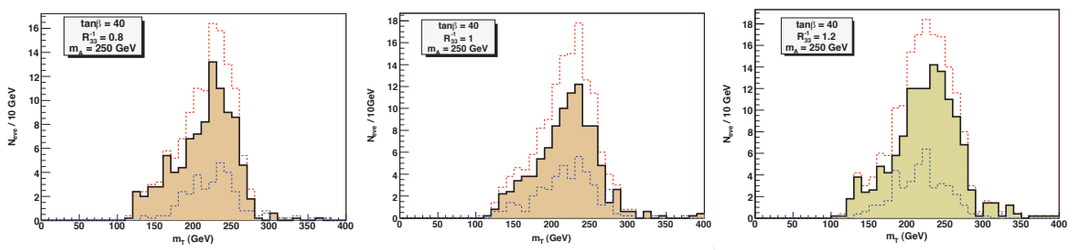

Fig. 5. Plots of the transverse mass of the charged Higgs in $H \to \tau\nu$ for a luminosity of 300fb^{-1} scaled to 30fb^{-1}. The three lines in each plot correspond to positive events (the dotted red lines), negative events (dotted and blue) and matched events (shaded portion and black). The three graphs corresponds to three different values of R^{-1} as indicated in each plot.

where $b'(x, \mu_F^2)$ is the leading order b-quark density given by [22]:

$$b'(x, \mu_F^2) \approx \frac{\alpha_s}{2\pi} \log \frac{\mu_F^2}{m_b^2} \int \frac{dz}{z} P_{qg}(z)\, g\left(\frac{x}{z}, \mu_F^2\right) , \tag{23}$$

with P_{qg} the $g \to q\bar{q}$ splitting function, $g(x, \mu_F^2)$ the gluon density function, μ_F the factorization scale and z the longitudinal gluon momentum fraction taken by the b-quark.

Including kinematic constraints due to finite center of mass energy (CM) and finite b quark mass, the resulting expression for the double-counting term can be written as [24]:

$$\sigma_{\rm DC} = \int_{\tau_{\rm min}}^{1} \frac{d\tau}{\tau} \int_{\frac{1}{2}\log\tau}^{-\frac{1}{2}\log\tau} dy^* \frac{\pi}{\widehat{s}} \int_{-1}^{1} \frac{\beta_{34}}{2} d(\cos\widehat{\theta})\, |\mathcal{M}_{2\to2}|^2 \frac{\alpha_s(\mu_R^2)}{2\pi}$$
$$\times \left[\int_{x_1}^{z_{\rm max}} dz P_{qg}(z) \int_{Q^2_{\rm min}}^{Q^2_{\rm max}} \frac{d(Q^2)}{Q^2 + m_b^2} \frac{x_1}{z} g\left(\frac{x_1}{z}, \mu_F^2\right) x_2 g(x_2, \mu_F^2) + x_1 \leftrightarrow x_2 \right] . \tag{24}$$

Here $\mathcal{M}_{2\to2}$ is the matrix element for the $g\bar{b} \to tH^{\pm}$ process, μ_F and μ_R are the factorization and renormalization scales as in the $gg \to t\bar{b}H^{\pm}$ process, and the kinematical variables are $\tau = x_1 x_2$, $x_{1,2} = \sqrt{\tau} e^{\pm y^*}$, $\widehat{s} = \tau s$. $\widehat{\theta}$ is the polar angle of the t-quark in the CM system of the $g\bar{b} \to tH^{\pm}$ scattering, and $\beta_{34} = \widehat{s}^{-1}\sqrt{(\widehat{s} - m_t^2 - m_{H^{\pm}}^2)^2 - 4m_t^2 m_{H^{\pm}}^2}$. Q^2 is the virtuality of the incoming b-quark and z is identified with the ratio of the CM energies of the gb system and the gg system.

Note that since the double-counting contribution should be subtracted from the sum of the positive processes, this weight is negative for double-counting events. This means that if all three processes are run simultaneously in PYTHIA, the total cross-section will be correctly matched.

With use of MATCHIG, issues of double-counting in our event generator are resolved. However, we shall not use the Monte-Carlo event generator, PYTHIA, to calculate the precise normalisation of the cross-sections, for though it gives an accurate description of the simulated data in both the low and high transverse momenta regions (with the inclusion of the external process MATCHIG), we can more accurately determine these by taking the leading order cross-section multiplied by an appropriate k-factor. The reason for this is that the matched

sum is still normalised to the LO total cross-section, we renormalise it to NLO precision using CTEQ6M parton densities and the corresponding value of $\lambda_{\overline{\rm MS}}^{n_f=5} = 226$ MeV in the computations given in Ref.[25, 26], which has been shown to be in good agreement with the one performed in Ref.[27]. For a Higgs boson mass of 300 GeV and in the $\tan\beta$ region of 30–50 considered here, the correction varies very little and can be well approximated with a constant factor of 1.2.

3.2 Simulations of the $H^\pm \to \tau\nu$ decay mode

As has already been mentioned, the $\tau\nu$ decay channel offers a high transverse momenta, p_T, of the τ and a large missing energy signature that can be discovered at the LHC over a vast region of the parameter space, where constraints have already been determined [17, 18]. To simulate this the events were generated in PYTHIA using the $gb \to tH^\pm$ process, explicitly using the mechanism $pp \to t(b)H^\pm \to jjb(b)\tau\nu$. That is, the associated top quark is required to decay hadronically, $t \to jjb$. The charged Higgs decays into a τ lepton, $H^\pm \to \tau^\pm\nu_\tau$, and the hadronic decays of the τ are considered. The backgrounds considered are QCD, $W+$ jets, single top production Wt, and $t\bar{t}$, with one $W \to jj$ and the other $W^\pm \to \tau^\pm\nu_\tau$.

The width of the process $H^\pm \to \tau^\pm\nu_\tau$ is:

$$\Gamma(H^- \to \tau^-\nu_\tau) \simeq \frac{m_{H^\pm}}{8\pi v^2}\left[m_\tau^2 \tan^2\beta\left(1-\frac{m_\tau^2}{m_{H^\pm}^2}\right)\right]\left(1-\frac{m_\tau^2}{m_{H^\pm}^2}\right) . \tag{25}$$

If the decay $H^\pm \to tb$ is kinematically allowed, comparing its width with Eq.(25) can give a rough estimate of the $H^\pm \to \tau^\pm\nu_\tau$ branching ratio:

$$\begin{aligned} Br(H^\pm \to \tau^\pm\nu_\tau) &\simeq \frac{\Gamma(H^\pm \to \tau^\pm\nu_\tau)}{\Gamma(H^\pm \to tb) + \Gamma(H^\pm \to \tau^\pm\nu_\tau)} \\ &= \frac{m_\tau^2 \tan^2\beta}{3(R_t^{-1})^2(m_t^2\cot^2\beta + m_b^2\tan^2\beta) + m_\tau^2\tan^2\beta} . \end{aligned} \tag{26}$$

Note that a measurement of the signal rate in $H^\pm \to \tau^\pm\nu_\tau$ can allow a determination of $\tan\beta$.

Our approach for this process is as follows:

- We first searched for events having one τ jet, two light non-τ jets and at least one (or two) b-jets. There is no isolated hard lepton in this configuration.
- A W-boson from the top quark decay was first reconstructed using a light jet pair. Note that we retained all the combinations of light jets that satisfy $|m_{jj} - m_W|^2 < 25$GeV. We then rescaled the four momenta of such jets in order to arrive at the correct W-boson mass.
- We then reconstructed the top quark by pairing the above constructed W-boson with the bottom quarks. Choosing the combination which minimises $\chi^2 = (m_{jjb} - m_t)^2$, we only retained the events that satisfied $|m_{jjb} - m_t| < 25$GeV.
- In this case, due to the presence of missing energy (the neutrino) in the charged Higgs decay, we can not reconstruct the charged Higgs mass. Instead we constructed the transverse mass of the charged Higgs.

Note that we were required to impose additional cuts, namely:

- $\mathcal{N}_1$: On the transverse momenta, $p_T > 100$GeV. A hard cut that allows events for a more massive charged Higgs bosons to pass through. This cut is satisfied by the events that originate from W with large p_T. This cut is severe for relatively light charged Higgs bosons (up to 200GeV) as it removes a large number of events, but is a very good cut for a relatively heavy Higgs.
- $\mathcal{N}_2$: On the missing transverse momenta, $p_T^{miss} > 100$GeV. Another hard cut which removes any possible QCD backgrounds, as typically QCD events have no hard leptons. Again this cut is problematic for relatively light Higgs masses, as it removes a large number of events.
- $\mathcal{N}_3$: Finally, a cut on the azimuthal angle between p_T and p_T^{miss} was made. This cut removes the events coming from W with large p_T. The decay product of such high p_T W-bosons will satisfy the cuts on p_T^{τ} and p_T^{miss} as defined above. Such events originating from large p_T W-bosons gives a large boost to the final products, and hence forces a rather small opening in the angle between the τ and ν. In the case of the charged Higgs (whose mass is much greater than the W's) the boost is relatively smaller, and this gives a relatively large angle between the τ and ν. As such we cut the azimuthal angle for $\delta\phi > 1$ rad. This cut becomes much more effective as we move to larger Higgs masses, as the Lorentz boost for larger masses is much less, and hence there shall be larger angles between the final products.

Note also, that in order to add a greater degree of realism to our analysis we have also required that the:

- B-tagging efficiency be 60%.
- c-jets being misidentified as b-jets at 10%.
- light jets be misidentified as b-jets at 3%.
- τ jet tagging efficiency be 70%,

which is somewhat more optimistic than current ATLAS results [17].

In Fig.5 we have plotted the transverse mass of the charged Higgs in the $H \to \tau\nu$ decay for a luminosity of $300fb^{-1}$, scaled to $30fb^{-1}$. In the plot the three lines correspond to positive events (where all three subprocesses are considered together), negative events (the amount to be subtracted to avoid double-counting) and the final matched events. The three panels correspond to different values of R^{-1}, as indicated. From this it can be observed that the resonance just below 250GeV is not particularly sensitive to the value of R^{-1}, the height of peak is slightly larger for higher values of R^{-1}. To further demonstrate the value of this process, we present in table 1 a comparison of the number of signal to background events, where the uncertainty in cross-section measurements is estimated as [10]:

$$\frac{\triangle(\sigma \times BR)}{(\sigma \times BR)} = \sqrt{\frac{S+B}{S^2}}\,,$$

where S and B are signal and background events respectively.

The numerical results of our analysis are therefore summarized in table 1. The table shows that for a reasonable range of input parameters the cross-sections at the LHC can be measured with a 10% accuracy for a luminosity of $\mathcal{L}$ = 100 fb^{-1}, whereas the measurement can be improved substantially for higher luminosities. Note that the error in the measurement of $\tan\beta$ is consistent with the observations made in Ref.[10]. For our analysis we have taken the

	$R_{33}^{-1} = 0.7$	$R_{33}^{-1} = 1$	$R_{33}^{-1} = 1.3$
σ (fb)	204	249	273
Pre-selection	48×10^{-3}	48×10^{-3}	48×10^{-3}
$\mathcal{N}_1$	12.8×10^{-3}	13×10^{-3}	13×10^{-3}
$\mathcal{N}_2$	61×10^{-4}	67×10^{-4}	66×10^{-4}
$\mathcal{N}_3$	47×10^{-4}	53×10^{-4}	52×10^{-4}
$\triangle(\sigma \times \text{BR}) / (\sigma \times \text{BR})$ ($\mathcal{L} = 100 fb^{-1}$)	10.6 %	9.5 %	8.6 %
$\triangle(\sigma \times \text{BR}) / (\sigma \times \text{BR})$ ($\mathcal{L} = 300 fb^{-1}$)	6.2 %	5.5 %	5 %

Table 1. Cumulative efficiencies of cuts and estimated errors for measurements of a signal cross-section for the process $pp \to t(b)H(\to \tau^{had}\nu)$. For these numbers we have fixed $m_{H^\pm} = 300$ GeV.

error in the measurement of the cross-section in this channel to be 10% for a luminosity of 100 fb^{-1} and 7.5% for a luminosity of 300 fb^{-1}. At this point we would like to note that for our results we have used fast detector simulator ATLFAST [28] and have followed the methodology as given in Ref.[10].

3.3 Simulations of the $H^\pm \to tb$ decay mode

Finally, for the decay chain $H^\pm \to tb$, recall that the interaction term of the charged Higgs with the t and b quarks in the 2HDM of type II, as given by Ref.[10], is:

$$\mathcal{L} = \frac{g(R_{33}^{-1})^{-1}}{2\sqrt{2}\, m_W} V_{tb} H^+ \bar{t} \left(m_t \cot\beta(1-\gamma_5) + m_b \tan\beta(1+\gamma_5)\right) b + h.c. \,. \tag{27}$$

For the hadroproduction process $gb \to tH^\pm$ (see Fig.3) with the decay mechanism $H^\pm \to tb$, the cross section for $gb \to tH^\pm$ can be written as:

$$\sigma(gb \to tH^\pm) \propto (R_{33}^{-1})^{-2} \left(m_t^2 \cot^2\beta + m_b^2 \tan^2\beta\right) \,. \tag{28}$$

Therefore, the decay width of $H^- \to \bar{t}b$ is given by:

$$\Gamma(H^- \to \bar{t}b) \simeq \frac{3\, m_{H^\pm}(R_{33}^{-1})^{-2}}{8\,\pi v^2} \Big[\left(m_t^2 \cot^2\beta + m_b^2 \tan^2\beta\right) \left(1 - \frac{m_t^2}{m_{H^\pm}^2} - \frac{m_b^2}{m_{H^\pm}^2}\right) - \frac{4 m_t^2 m_b^2}{m_{H^\pm}^2} \Big] \times \left[1 - \left(\frac{m_t + m_b}{m_{H^\pm}}\right)^2\right]^{1/2} \left[1 - \left(\frac{m_t - m_b}{m_{H^\pm}}\right)^2\right]^{1/2} , \tag{29}$$

where the factor 3 takes into account the number of colours. The final state of the hadroproduction process contains two top quarks, one of which we required to decay semi-leptonically to provide the trigger, $t \to \ell\nu b$ ($\ell = e,\ \mu$), and the other hadronically, $\bar{t} \to jjb$. The main background comes from $t\bar{t}b$ and $t\bar{t}q$ production with $t\bar{t} \to WbWb \to \ell\nu bjjb$.

As such, we have used the production channel $pp \to tH^\pm$ for this decay, and have tried to reconstruct the charged Higgs mass. That is, we have the following decay chain:

$$pp \to tH^\pm \to t(tb) \to (\ell\nu_\ell b)(jjb)b \to \ell jjbbb\nu \,. \tag{30}$$

The procedure we have used in reconstructing the masses is:

- We initially searched for one isolated lepton (both electrons and muons) with at least three tagged b-jets (this is done in order to include processes like $gg \to tbH$) and at least two non b-jets. Furthermore, we used the cuts, where for b and non-b jets we used the same p_T cuts, $p_T^e > 20\text{GeV}$, $p_T^\mu > 6\text{GeV}$, $p_T^j > 30\text{GeV}$ and $|\eta| < 2.5$.
- Next we tried to reconstruct the W mass (where the W originates from the top decay) in both leptonic ($W \to \ell\nu$) and hadronic ($W \to jj$) decays. For the leptonic decay we attributed the missing p_T to the emergence of neutrinos from the leptonic W decay. Using the actual W mass we then reconstructed the longitudinal neutrino momentum. This gives a two fold ambiguity, both corresponding to the actual W mass, and neglecting the event if it gives an unphysical solution. Choosing both solutions the second W is reconstructed in the jet mode. We constructed all possible combinations of non-b jets and have plotted the invariant mass of the jets (m_{jj}), retaining only those combinations of jets which are consistent with $|m_{jj} - m_W| < 10\text{GeV}$. Note that the rescaling is done by scaling the four momenta of the jets with the W mass, that is, $p'_j = p_j \times m_W / m_{jj}$.
- We then attempted to reconstruct the top quarks, where we have, at present, reconstructed two W bosons and three tagged b jets. There can be six different combinations of W's and b-jets that can give top quarks. As such, we chose the top quarks which minimise

$$(m_{jjb} - m_t)^2 + (m_{\ell\nu b} - m_t)^2 \, .$$

- Finally, we retained the top quarks that satisfy $|m_{jjb} - m_t| < 12\text{GeV}$ and $|m_{\ell\nu b} - m_t| < 12\text{GeV}$. This leaves two top quarks and one b-jet. There can be two possible combinations, where we retained both. It should be noted that only one of the combinations is the true combination (the combination that emerged from a charged Higgs), the other combination being combinatorial backgrounds.

Using these techniques we can now generate the correlation plot of the two LHC processes considered here, see Fig.6. In these plots we have considered three different values of R_{33}^{-1}, where these lines of constant R_{33}^{-1} are generated from three values of $\tan\beta$ (that is, $\tan\beta = 30, 40$ and 50). Note that though this mode has a much larger branching ratio than $H^\pm \to \tau\nu$, it has at least three b-jets in its final state. As such, the combinatorial backgrounds associated with this channel make it a challenging task to work with [10], and not the best discovery channel for a charged Higgs at the LHC.

4. Charged Higgs at B-factories

Having now reviewed how a massive charged Higgs may be detected at the LHC, we shall now place greater constraints on the charged Higgs parameters by utilising the successful B factory results from KEK and SLAC. Note that B physics shall be a particularly fertile ground to place constraints on a charged Higgs. For example, it is well known that limits from $b \to s\gamma$ can give stronger constraints in generic 2HDMs than in SUSY models [29]!

The B decays of most interest here are those including a final τ particle, namely $B \to D\tau\nu$ and $B \to \tau\nu$[8]. An important feature of these processes is that a charged Higgs boson can contribute to the decay amplitude at tree-level in models such as the 2HDM and the MSSM. From the experimental perspective, since at least two neutrinos are present in the final state (on the signal side), a full-reconstruction is required for the B decay on the opposite side. For the $B \to D\tau\nu$ process, the branching fraction has been measured at BaBar with

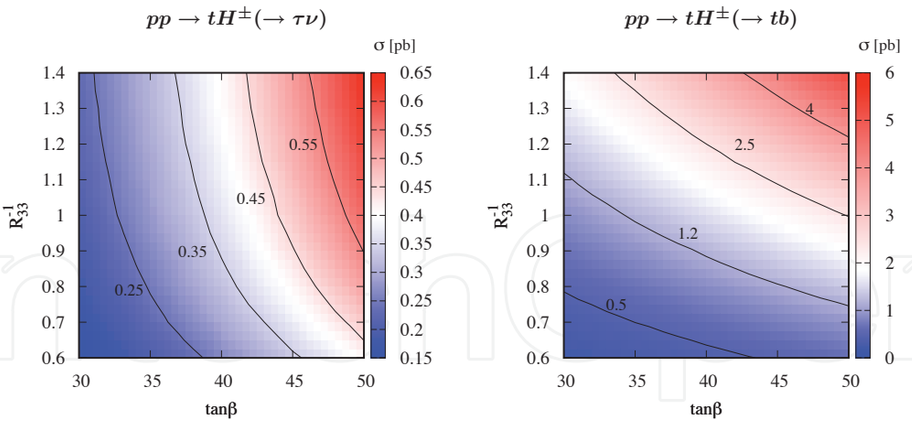

Fig. 6. Contour plots of the cross-sections for the processes $pp \to tH^{\pm}(\to \tau\nu)$ (left) and $pp \to tH^{\pm}(\to tb)$ (right) versus R_{33}^{-1} and $\tan\beta$ with fixed $m_{H^{\pm}}$ =300 GeV [11].

$Br(B \to D^{+}\tau^{-}\bar{\nu}_{\tau}) = 0.86 \pm 0.24 \pm 0.11 \pm 0.06\%$ [30], which is consistent, within experimental uncertainties, with the SM, and with Belle [31]. Note also that the inclusive $b \to c\tau\nu$ branching ratio was determined at the LEP experiments [32]. The $B \to \tau\nu$ process has a smaller branching ratio, as measured by Belle at $(1.79\ ^{+0.56}_{-0.49}\ (stat)\ ^{+0.46}_{-0.51}\ (syst)) \times 10^{-4}$ [33], and at BaBar $(1.2 \pm 0.4 \pm 0.3 \pm 0.2) \times 10^{-4}$ [34] (giving an average of $(1.41\ ^{+0.43}_{-0.42}) \times 10^{-4}$ [35]). Note that the SM predicts $Br(B \to \tau\nu) = (7.57\ ^{+0.98}_{-0.61}) \times 10^{-5}$, where theoretical uncertainties came from f_B, the B meson decay constant, which from lattice QCD is $f_B = 191 \pm 13$ MeV. As such, the measurement of these processes will be important targets in coming B factory experiments.

In order to test for the charged Higgs fermion couplings, we now determine the charged Higgs contributions to tauonic B decays, where it is straightforward to write down the amplitudes for the $B \to D\tau\nu$ ($B^{-} \to \overline{D}^{0}\tau^{-}\overline{\nu}$ or $\overline{B}^{0} \to D^{+}\tau^{-}\overline{\nu}$) and $B \to \tau\nu$ processes. We should first like to note that the higgsino diagram contributions, see Fig.1(a), to the R_{22}^{-1} are proportional to square of the charm Yukawa couplings, and since the branching ratio can change only by at most a few percent, we shall neglect such contributions here. Also, as we shall work with large $\tan\beta$ values, $\cot\beta$ terms can be neglected in the Lagrangian.

We can now calculate the charged Higgs effect on the $B \to D\tau\nu$ branching ratio, by utilising the vector and scalar form factors of the $B \to D$ transition. These are obtained using the effective Lagrangian for $b \to c\tau\nu$ operators as given by

$$\mathcal{L}_{\text{eff}} = -\frac{G_{\text{F}}}{\sqrt{2}} V_{cb}\bar{c}\gamma_{\mu}(1-\gamma_5)b\overline{\tau}\gamma^{\mu}(1-\gamma_5)\nu_{\tau} + G_{\text{S}}\bar{c}b\overline{\tau}(1-\gamma_5)\nu_{\tau} + G_{\text{P}}\bar{c}\gamma_5 b\overline{\tau}(1-\gamma_5)\nu_{\tau} + \text{h.c.}\,, \quad (31)$$

where G_{S} and G_{P} are scalar and pseudo-scalar effective couplings. These couplings are given from Eqs.(10), (11) and the similarly derived effective Lagrangian for charged leptons:

$$G_{\text{S}} \equiv \frac{\tan^2\beta M_{\tau}}{2v^2 M_{H^{\pm}}^2}[\hat{R}_e^{-1}]_{33}(M_b[\hat{R}_d^{-1}]_{22}V_{cb} + M_c V_{cb}\cot^2\beta)\,, \quad (32)$$

$$G_{\text{P}} \equiv \frac{\tan^2\beta M_{\tau}}{2v^2 M_{H^{\pm}}^2}[\hat{R}_e^{-1}]_{33}(M_b[\hat{R}_d^{-1}]_{22}V_{cb} - M_c V_{cb}\cot^2\beta)\,, \quad (33)$$

where we shall now omit a prime from the fields in mass eigenstates. Recall that we shall neglect higgsino diagram contributions to the $[\hat{R}_d^{-1}]_{22}$ proportional to the square of the charm Yukawa couplings, and also neglect the last terms in G_S and G_P.

In the heavy quark limit, these form factors can be parameterized by a unique function called the Isgur-Wise function. From the semi-leptonic decays $B \to Dl\nu$ and $B \to D^* l\nu$ ($l = e, \mu$), the Isgur-Wise function is obtained in a one-parameter form, including the short distance and $1/M_Q$ ($Q = b, c$) corrections. The short distance corrections for $B \to D\tau\nu$ have also been calculated previously [36]. Here we adopt this Isgur-Wise function, but do not include the short distance and the $1/M_Q$ corrections for simplicity.

Using the definitions,

$$x \equiv \frac{2p_{B\cdot D}}{p_B^2}\ ,\ y \equiv \frac{2p_{B\cdot ø}}{p_B^2}\ ,\ r_D \equiv \frac{M_D^2}{M_B^2}\ ,\ r_ø \equiv \frac{M_ø^2}{M_B^2}\ , \tag{34}$$

the differential decay width is given by

$$\frac{d^2\Gamma[B \to D\tau\nu]}{dxdy} = \frac{G_F^2|V_{cb}|^2}{128\pi^3} M_B^5 \rho_D(x,y)\ , \tag{35}$$

where

$$\begin{aligned}
\rho_D(x,y) &\equiv [|f_+|^2 g_1(x,y) + 2\mathrm{Re}(f_+ f_-'^*) g_2(x,y) + |f_-'|^2 g_3(x)]\ , \\
g_1(x,y) &\equiv (3 - x - 2y - r_D + r_ø)(x + 2y - 1 - r_D - r_ø) - (1 + x + r_D)(1 + r_D - r_ø - x)\ , \\
g_2(x,y) &\equiv r_ø(3 - x - 2y - r_D + r_ø)\ , \\
g_3(x) &\equiv r_ø(1 + r_D - r_ø - x)\ , \\
f_-' &\equiv \{f_- - \Delta_S[f_+(1 - r_D) + f_-(1 + r_D - x)]\}\ , \\
f_\pm &= \pm\frac{1 \pm \sqrt{r_D}}{2\sqrt[4]{r_D}}\xi(w),\ \ (w = \frac{x}{2\sqrt{r_D}})\ .
\end{aligned}$$

Here $\Delta_S \equiv \frac{\sqrt{2}G_S M_B^2}{G_F V_{cb} M_\tau (M_b - M_c)}$. We use the following form of the Isgur-Wise function.

$$\begin{aligned}
\xi(w) &= 1 - 8\rho_1^2 z + (51\rho_1^2 - 10)z^2 - (252\rho_1^2 - 84)z^3\ , \\
z &= \frac{\sqrt{w+1} - \sqrt{2}}{\sqrt{w+1} + \sqrt{2}}\ .
\end{aligned}$$

For the slope parameter we use $\rho_1^2 = 1.33 \pm 0.22$ [36, 37].

Similarly, for the $B \to \tau\nu$ process, the relevant four fermion interactions are those of the $b \to u\tau\nu$ type [8]:

$$\mathcal{L}'_{\mathrm{eff}} = -\frac{G_F}{\sqrt{2}} V_{ub}\bar{u}\gamma_\mu(1 - \gamma_5)b\bar{\tau}\gamma^\mu(1 - \gamma_5)\nu_\tau + G'_S\bar{u}b\bar{\tau}(1 - \gamma_5)\nu_\tau + G'_P\bar{u}\gamma_5 b\bar{\tau}(1 - \gamma_5)\nu_\tau + \mathrm{h.c.}\ , \tag{36}$$

$$G'_S \equiv \frac{\tan^2\beta M_\tau}{2v^2 M_{H^\pm}^2}[\hat{R}_e^{-1}]_{33}(M_b[\hat{R}_d^{-1}]_{11} V_{ub} + M_u V_{ub}\cot^2\beta)\ , \tag{37}$$

$$G'_P \equiv \frac{\tan^2\beta M_\tau}{2v^2 M_{H^\pm}^2}[\hat{R}_e^{-1}]_{33}(M_b[\hat{R}_d^{-1}]_{11} V_{ub} - M_u V_{ub}\cot^2\beta)\ . \tag{38}$$

Using the matrix elements

$$\langle 0|\overline{u}\gamma^{\mu}\gamma_5 b|B^-\rangle = if_{\rm B}p^{\mu}\ ,$$
$$\langle 0|\overline{u}\gamma_5 b|B^-\rangle = -if_{\rm B}\frac{M_{\rm B}^2}{M_b}\ ,$$

the decay width of $B \to \tau\nu$ in the SM is given by:

$$\Gamma[B\to\tau\nu_\tau]_{SM} = \frac{G_F^2}{8\pi}|V_{ub}|^2 f_B^2 m_\tau^2 m_B\left(1-\frac{m_\tau^2}{m_B^2}\right)^2, \tag{39}$$

which in the presence of a charged Higgs boson, is modified by a multiplicative factor to:

$$\Gamma[B\to\tau\nu_\tau]_{2HDM} = \Gamma[B\to\tau\nu_\tau]_{SM}\times\left(1-\frac{m_B^2}{m_{H^\pm}^2}\tan^2\beta\right)^2, \tag{40}$$

in the effective limits we have adopted. Note that our input parameters are the projected values for Super$B$, that is, we shall use $f_{\rm B} = 200 \pm 30$MeV in our numerics.

Note that this link can be understood by recalling that in our generalized case of MFV, that is Eq.(16), the scalar and pseudo-scalar couplings, Eqs.(32), (33), (37), and (38) can be obtained by the following replacement.

$$[\hat{R}_d^{-1}]_{22} \to \frac{1}{1+[E_{\widetilde{g}}^{(3)} - E_{\widetilde{g}}^{\prime\,(32)}]\tan\beta}, \tag{41}$$

$$[\hat{R}_d^{-1}]_{11} \to \frac{1}{1+[E_{\widetilde{g}}^{(3)} - E_{\widetilde{g}}^{\prime\,(31)}]\tan\beta}\ , \tag{42}$$

where $E_{\widetilde{g}}^{(i)}$ and $E_{\widetilde{g}}^{\prime\,(ij)}$ were defined in section 2.1. Notice that the right-handed sides of the above equations are approximately the same because $E_{\widetilde{g}}^{\prime\,(31)} \approx E_{\widetilde{g}}^{\prime\,(32)}$. This is the generalization of $[\hat{R}_d^{-1}]_{11} \approx [\hat{R}_d^{-1}]_{22}$, which follows from fact that the higgsino diagram contribution can be neglected in the evaluation with the $[\hat{R}_d^{-1}]_{11}$ and $[\hat{R}_d^{-1}]_{22}$.

Using these results we have generated the contour plots in Fig.7(b), where a correlation of the $B \to D\tau\nu$ ($B^- \to \overline{D}^0\tau^-\overline{\nu}$ or $\overline{B}^0 \to D^+\tau^-\overline{\nu}$) and $B \to \tau\nu$ branching ratios for various values of $\tan\beta$ and $\widehat{R}_d^{-1}$ and $m_{H^\pm} = 300$GeV, have been given.

5. Determination of the effective couplings

Collecting our numerical results from section 3 and the branching ratios calculated in the previous subsection, we have generated the plots in Figs.7 and 8. In these figures we can see correlations of the LHC cross-sections with the two B processes, where in these plots we have varied $\tan\beta$ in the range $30 < \tan\beta < 50$ for different values of R_{ii}^{-1} ($ii = 11, 33$). Fig.7(a) shows the correlation of the LHC observables, whilst the correlation of B-decay branching ratios in Fig.7(b) gives the same line for different values of R_{11}^{-1}. The reason for this can be seen from Eq.(36) where R_{ii}^{-1} and $\tan\beta$ arise from the same combination ($\equiv R_{ii}^{-1}\tan^2\beta$) in

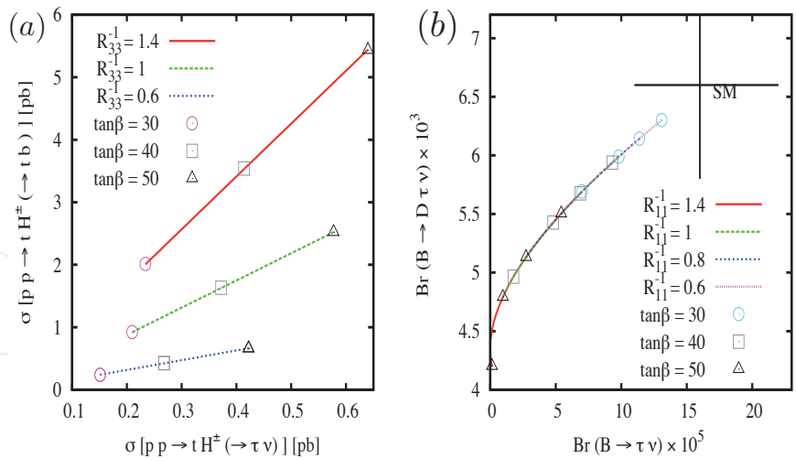

Fig. 7. Correlation plots of the cross-sections for the processes $pp \to t(b)H^{\pm}(\to \tau\nu)$ and $pp \to t(b)H^{\pm}(\to tb)$ for three values of R_{33}^{-1} and $\tan\beta$ (left) and of the branching ratios for $B \to D\tau\nu$ and $B \to \tau\nu$ (right) for various values of $\tan\beta$ and $\widehat{R}_d^{-1}$ with fixed $m_{H^{\pm}} = 300$ GeV [11].

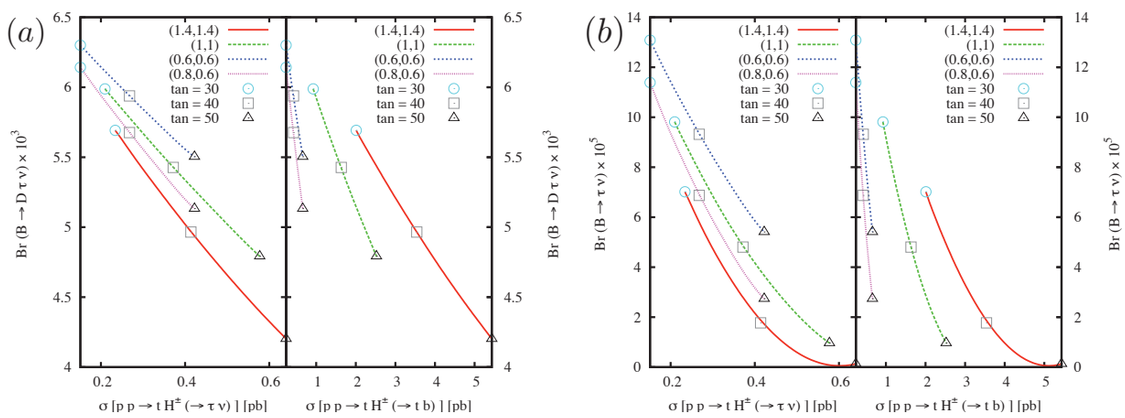

Fig. 8. Contour plots of the $B \to D\tau\nu$ branching ratio correlated with the cross-section $\sigma(pp \to t(b)H^{\pm}(\to \tau\nu)$ (a) left) and $\sigma(pp \to t(b)H^{\pm}(\to tb)$ (a) right), and the $B \to \tau\nu$ branching ratio correlated with the cross-section $\sigma(pp \to t(b)H^{\pm}(\to \tau\nu)$ (b) left) and $\sigma(pp \to t(b)H^{\pm}(\to tb)$ (b) right), for various values of $\tan\beta$ and R^{-1} (the bracketed numbers in the key refer to the appropriate R^{-1} for each process being considered)[11].

the tauonic B-decays considered in this work. Hence the measurement of these two B-decays will only give an estimate of the product of R_{11}^{-1} and $\tan\beta$. However, by considering the correlations of the B-decay observables with LHC observables, as shown in Fig.8, one can remove this degeneracy. So in principle it is possible to measure the four parameters ($\tan\beta$ and R_{ii}^{-1} with $ii = 11, 22, 33$) using the six correlation plots shown in Figs.7 and 8.

The primary question to be answered in this effective test of the charged Higgs couplings is "to what precision can we test R^{-1}?". From our simulations we can safely assume that the LHC shall determine, to some level of precision, values for $m_{H^{\pm}}$ and/or $\tan\beta$. These values can then be converted into a value for R^{-1} with all the precision afforded to us from

the results of the B-factory experiments, as demonstrated pictorially in Fig.8. Assuming the charged Higgs boson mass to be known (taken to be 300 GeV in our present analysis) we have obtained cross-section measurement uncertainties as given in table 1. As can be seen from this, it might be possible to measure R_{33}^{-1} and $\tan\beta$ with an accuracy of about 10% at high luminosity. Armed with this information about $\tan\beta$, from the LHC measurements, it can then be taken as an input to the B-decay measurements, namely $B \to \tau\nu$ and $B \to D\tau\nu$. In Ref.[10] it was inferred that for large values of $\tan\beta$ (≥ 40), measurements to a precision of 6-7% for high luminosity LHC results are possible. Our results are consistent with these observations. Future Super-B factories are expected to measure the $B \to \tau\nu$ and $B \to D\tau\nu$ to a precision of 4% and 2.5% respectively [38]. The present world average experimental results for tauonic B-decays are $BR(B \to \tau\nu) = (1.51 \pm 0.33) \times 10^{-4}$ and $BR(B \to D\tau\nu)/BR(B \to D\mu\nu) = (41.6 \pm 11.7 \pm 5.2)\%$ [30, 38]. Presently if one uses UTfit prescription of $|V_{ub}|$ then there is substantial disagreement between experimental and SM estimates for the branching fractions of $B \to \tau\nu$. Recently, proposals have been given in Ref.[39] to reduce this tension between experimental and theoretical SM values of $B \to \tau\nu$. Transforming the improved projected theoretical information of these decays along with future Super-B factory measurements one can measure R_{11}^{-1} and R_{22}^{-1} to a fairly high precision.

To summarise, we have tried to demonstrate that at the LHC alone it is possible to measure the charged Higgs boson couplings, namely $\tan\beta$ and R_{33}^{-1}, to an accuracy of less than 10%. Combining this information from the LHC with improved B-factory measurements, one can measure all four observables indicated in the introduction. These observables represent effective couplings of a charged Higgs boson to the bottom quark and the three generations of up-type quarks, thus demonstrating that it is possible to test the charged Higgs boson couplings to quarks by the combination of low energy measurements at future Super-B factories and charged Higgs boson production at the LHC. Something which shall be realisable in the very near future as results from the LHC are already starting to emerge [17, 18], and which will require more refined analyses in the near future.

6. References

[1] P. Fayet and S. Ferrara, Phys. Rept. 32, 249 (1977); H.P. Nilles, Phys. Rep. 110, 1 (1984); H.E. Haber and G. L. Kane, Phys. Rep. 117, 75 (1985).
[2] S.L. Glashow and S. Weinberg, Phys. Rev. D15, 1958 (1977).
[3] H. Georgi and D.V. Nanopoulos, Phys. Lett. 82B, 95 (1979).
[4] H.E. Haber, G.L. Kane and T. Sterling, Nucl. Phys. B161, 493 (1979).
[5] L.J. Hall and M.B. Wise, Nucl. Phys. B187, 397 (1981).
[6] J.F. Donoghue and L.F. Li, Phys. Rev. D19, 945 (1979).
[7] W.S. Hou, Phys. Lett. B296, 179 (1992); D. Chang, W.S. Hou and W.Y. Keung, Phys. Rev. D48, 217 (1993); D. Atwood, L. Reina and A. Soni, Phys. Rev. D55, 3156 (1997).
[8] H. Itoh, S. Komine and Y. Okada, Prog. Theor. Phys. 114, 179 (2005) [arXiv:hep-ph/0409228].
[9] L. J. Hall, R. Rattazzi and U. Sarid, Phys. Rev. D 50, 7048 (1994).
[10] K. A. Assamagan, Y. Coadou and A. Deandrea, Eur. Phys. J. directC 4, 9 (2002) [arXiv:hep-ph/0203121].
[11] A. S. Cornell, A. Deandrea, N. Gaur, H. Itoh, M. Klasen, Y. Okada, Phys. Rev. D81, 115008 (2010).
[12] M. Gorbahn, S. Jäger, U. Nierste and S. Trine, arXiv:0901.2065 [hep-ph].

[13] T. Blazek, S. Raby and S. Pokorski, Phys. Rev. D 52, 4151 (1995).
[14] K. S. Babu and C. F. Kolda, Phys. Rev. Lett. 84, 228 (2000);
[15] [LEP Higgs Working Group for Higgs boson searches and ALEPH Collaboration], arXiv:hep-ex/0107031.
[16] V. M. Abazov *et al.* [D0 Collaboration], Phys. Lett. B 682, 278 (2009) [arXiv:0908.1811 [hep-ex]].
[17] The ATLAS Collaboration, ATLAS-CONF-2011-138 August 31, 2011.
[18] The CMS Collaboration, CMS PAS HIG-11-008 July 22, 2011.
[19] J. F. Gunion, H. E. Haber, F. E. Paige, W. K. Tung and S. S. Willenbrock, Nucl. Phys. B 294, 621 (1987); J. L. Diaz-Cruz and O. A. Sampayo, Phys. Rev. D 50, 6820 (1994).
[20] A. Krause, T. Plehn, M. Spira and P. M. Zerwas, Nucl. Phys. B 519, 85 (1998) [arXiv:hep-ph/9707430]; Y. Jiang, W. g. Ma, L. Han, M. Han and Z. h. Yu, J. Phys. G 24, 83 (1998) [arXiv:hep-ph/9708421]; A. A. Barrientos Bendezu and B. A. Kniehl, Nucl. Phys. B 568, 305 (2000) [arXiv:hep-ph/9908385]; O. Brein and W. Hollik, Eur. Phys. J. C 13, 175 (2000) [arXiv:hep-ph/9908529].
[21] D. A. Dicus, J. L. Hewett, C. Kao and T. G. Rizzo, Phys. Rev. D 40, 787 (1989); A. A. Barrientos Bendezu and B. A. Kniehl, Phys. Rev. D 59, 015009 (1999) [arXiv:hep-ph/9807480]; Phys. Rev. D 61, 097701 (2000) [arXiv:hep-ph/9909502]; Phys. Rev. D 63, 015009 (2001) [arXiv:hep-ph/0007336]; O. Brein, W. Hollik and S. Kanemura, Phys. Rev. D 63, 095001 (2001) [arXiv:hep-ph/0008308].
[22] J. Alwall, arXiv:hep-ph/0503124.
[23] T. Sjöstrand, S. Mrenna and P. Skands, JHEP 0605, 026 (2006).
[24] J. Alwall and J. Rathsman, "Improved description of charged Higgs boson production at hadron colliders," JHEP 0412 (2004) 050 [arXiv:hep-ph/0409094].
[25] T. Plehn, Phys. Rev. D 67, 014018 (2003).
[26] E. L. Berger, T. Han, J. Jiang and T. Plehn, Phys. Rev. D 71, 115012 (2005).
[27] S. H. Zhu, Phys. Rev. D 67 075006 (2003).
[28] E. Richter-Was *et al.* , *ATLFAST 2.2: A fast simulation package for ATLAS*, ATL-PHYS-98-131.
[29] R. Bose and A. Kundu, arXiv:1108.4667 [hep-ph].
[30] B. Aubert *et al.* [BABAR Collaboration], Phys. Rev. Lett. 100, 021801 (2008) [arXiv:0709.1698 [hep-ex]].
[31] K. Abe *et al.* [Belle Collaboration], Phys. Lett. B 526, 258 (2002) [arXiv:hep-ex/0111082].
[32] G. Abbiendi *et al.* [OPAL Collaboration], Phys. Lett. B 520 (2001), 1; R. Barate *et al.* [ALEPH Collaboration], Eur. Phys. J. C 19 (2001), 213.
[33] K. Ikado *et al.*, Phys. Rev. Lett. 97, 251802 (2006) [arXiv:hep-ex/0604018].
[34] B. Aubert *et al.* [BABAR Collaboration], Phys. Rev. D 77, 011107 (2008) [arXiv:0708.2260 [hep-ex]]; B. Aubert *et al.* [BABAR Collaboration], Phys. Rev. D 76, 052002 (2007) [arXiv:0705.1820 [hep-ex]].
[35] Heavy Flavour Averaging Group, http://www.slac.stanford.edu.au/xorg/hfag/.
[36] T. Miki, T. Miura and M. Tanaka, in Shonan Village 2002, Higher luminosity B factories, arXiv:hep-ph/0210051.
[37] C. G. Boyd, B. Grinstein and R. F. Lebed, Phys. Rev. D 56 (1997), 6895; I. Caprini, L. Lellouch and M. Neubert, Nucl. Phys. B 530 (1998), 153.
[38] T. Browder, M. Ciuchini, T. Gershon, M. Hazumi, T. Hurth, Y. Okada and A. Stocchi, JHEP 0802, 110 (2008);
[39] E. Lunghi and A. Soni, arXiv:0912.0002 [hep-ph];

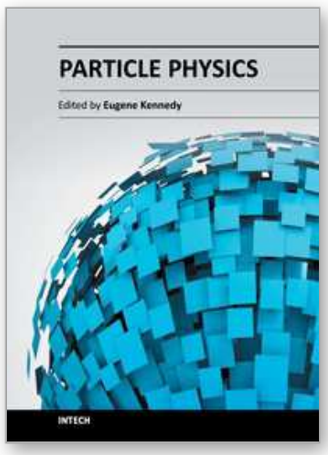

Particle Physics

Edited by Dr. Eugene Kennedy

ISBN 978-953-51-0481-0
Hard cover, 114 pages
Publisher InTech
Published online 20, April, 2012
Published in print edition April, 2012

Stimulated by the Large Hadron Collider and the search for the elusive Higgs Boson, interest in particle physics continues at a high level among scientists and the general public. This book includes theoretical aspects, with chapters outlining the generation model and a charged Higgs boson model as alternative scenarios to the Standard Model. An introduction is provided to postulated axion photon interactions and associated photon dispersion in magnetized media. The complexity of particle physics research requiring the synergistic combination of theory, hardware and computation is described in terms of the e-science paradigm. The book concludes with a chapter tackling potential radiation hazards associated with extremely weakly interacting neutrinos if produced in copious amounts with future high-energy muon-collider facilities.

INTECH
open science | open minds

InTech Europe
University Campus STeP Ri
Slavka Krautzeka 83/A
51000 Rijeka, Croatia
Phone: +385 (51) 770 447
Fax: +385 (51) 686 166
www.intechopen.com

InTech China
Unit 405, Office Block, Hotel Equatorial Shanghai
No.65, Yan An Road (West), Shanghai, 200040, China
中国上海市延安西路65号上海国际贵都大饭店办公楼405单元
Phone: +86-21-62489820
Fax: +86-21-62489821

IntechOpen